Influence of Patterning in the Acid-Base Interfacial Properties of Homogeneously Mixed CH_3- and COOH-Terminated Self-Assembled Monolayers

Alain R. Puente Santiago, Guadalupe Sánchez-Obrero, Teresa Pineda, Manuel Blázquez, and Rafael Madueño*

Departamento de Química Física y Termodinámica Aplicada, Instituto Universitario de Investigación en Química Fina y Nanoquímica IUIQFN, Facultad de Ciencias, Universidad de Córdoba, Campus de Rabanales, Ed. Marie Curie 2ª Planta, E-14071 Córdoba, España

AUTHOR E-MAIL ADDRESS

rafael.madueno@uco.es

CORRESPONDING AUTHOR FOOTNOTE

Phone number: +34-957-218646

Fax number: +34-957-218618

Abstract

The acid/base interfacial behavior of mixed self-assembled monolayers (SAMs) of 1-decanethiol (DT) and 11-mercaptoundecanoic acid (MUA) formed on gold from a micellar medium has been characterized by electrochemical impedance spectroscopy (EIS) and infrared reflection-absorption spectroscopy (IRRAS) titration experiments as a function of their surface composition. The surface composition is determined from the interfacial capacitance of the SAMs that behave as a dielectric medium of the expected thickness for well-organized layers. The interaction parameter, the apparent and the intrinsic surface pK_a values of these pH-responsive SAMs are obtained by fitting the EIS and IR titration curves to the 1-pK model. The shift in the surface pK_a while decreasing the MUA surface fraction resembles the behavior of homogenously mixed systems. The trends observed can be explained by the lowering of intermolecular in-plane repulsive interactions between neighboring MUA molecules, and by the local solvation and hydrophobic effects when the MUA domains decrease below a critical size and the terminal groups are probably titrated at domain boundaries, small arrangements or even isolated. The transition between both scenarios and the formation of hydrogen bonding interactions upon a structural reorganization is conditioned by the heterogeneity in the size distribution of MUA and DT molecular domains which depends on the formation conditions of the SAMs. All together is demonstrated to play a role in the acid/base properties of these monolayers which has a direct implication in the proper design of interfacial devices based on organic molecular junctions or biomolecular assemblies.

Introduction

Control in the spatial confinement of molecules and nano-objets on surfaces (i.e. surface patterning) is important for a wide variety of applications.[1, 2] In particular, the proper design of interfacial devices based on molecular and planar junctions is of special relevance in organic electronics, where tailoring of the surface chemistry by mixed self-assembled monolayers (SAMs) and the presence of structural defects in the molecular constituents has been demonstrated to play a crucial role in their electrical and thermal performance.[3-5] This fact allows to explore the behavior of organic electronic devices according to well-defined and tunable gradients of rectification while the local molecular environment affects the interfacial transport physics.[4, 5] The formation of patterns of molecularly mixed components with high structural order in a wide range of surface compositions, as we have recently reported for binary SAMs deposited from micellar media near to equilibrium conditions,[6] might meet such requirements.

Additionally, the composition, organization, thickness, conformation and mixing of the molecules in these multicomponent SAM surfaces not only determine their interfacial properties [7-9] but also modulate the activity and function of immobilized biomolecules and the stimuli responsive properties of biointerfaces (e.g. electrical, chemical, optical and thermal).[10-12] The control of the specific and non-specific adsorption of macromolecules at surfaces is of particular interest in prospect of designing biocompatible materials and developing new biosensing and biomedical applications.[13-19] In this sense, pure and mixed ω-alkanethiolate SAMs bearing pH-responsive ionisable end-groups is demonstrated to provide control in the surface distribution, orientation and density of proteins that can be immobilized on electrodes by mimicking electrostatic and non-electrostatic interactions of the biological milieu, and whose function as transducers can be consequently altered.[14, 15, 19-22] Non-covalent interactions are influenced by the

chemically and structurally-dependent interfacial properties of these pH-switchable SAMs, which are in turn affected by different factors determining their apparent surface pK_a such as the charge and polarity, hydrogen bonding effects, electrostatic fields and the local structure of the solvent in the vicinity of the terminal groups, among others. Therefore, fundamental knowledge of the acid-base properties of confined molecules as a function of their composition, organization and distribution within functionalized surfaces becomes necessary to develop the rational design of complex molecular assemblies.

This work aims to study the acid-base interfacial properties of 11-mercaptoundecanoic (MUA) and decanethiol (DT) pure and mixed SAMs formed on Au(111) surfaces from a lyotropic medium at low and high modification times. For this purpose, the titration of the terminal carboxyl groups exposed in the SAMs is characterized by electrochemical impedance spectroscopy (EIS) and infrared reflection-absorption spectroscopy (IRRAS), and the apparent surface pK_a values determined as a function of the MUA surface coverage. Interestingly, the different acid-base behavior found in these 2D-assemblies can be rationalized in terms of the structural organization of the layers and the spatial distribution of the –COOH groups according to their different mixing surface patterns and distribution of the domain sizes of the components. This fact has direct implication in the applications for which these SAMs are designed.

Experimental

Chemical reagents. MUA, DT, Triton X-100, $K_4Fe(CN)_6$, $K_3Fe(CN)_6$ and semiconductor grade purity KOH were purchased from Aldrich-Sigma (purity ≥ 99%). HCl, KNO_3, KCl and H_3PO_4 reagents were from Merck analytical grade. All solutions were prepared with deionized ultrapure water produced by a Millipore system.

Methods

Substrate cleaning. A conventional three electrode cell comprising a platinum coil as the counter electrode, a 50 mM KCl calomel electrode as the reference electrode (E = +0.353 V vs E^{o}_{NHE}) and Au(111) or polyfaceted gold bead surfaces as the working electrodes were used. Before each electrochemical and spectroscopic measurement, the gold surfaces were annealed in a natural gas flame and, after a short period of cooling in air, quenched in ultrapure water. Then, the electrode was transferred to the electrochemical cell with water adhered to it to prevent contamination and subsequently immersed in the electrolyte solution that was previously purged with N_2 (99.999%). The surface condition was confirmed by cyclic voltammetry (CV) in 0.01M $HClO_4$, [23] and the real surface area was determined from the integrated area of the reduction peak of oxygen adsorption on the Au electrodes.[24] This surface treatment was the most appropriate for producing unreconstructed surfaces that were clean, ordered and reproducible.[23]

SAMs´ formation and titration. The SAMs of MUA and/or DT were spontaneously formed by direct immersion of the clean substrates into a mixture of Triton X-100 (42%) and water (58%) to which the thiol derivatives were added at different mole ratios and a final concentration of 1 mM, as described elsewhere.[6] The adsorption times assayed in the mixtures were 15 minutes and 18 hours. The as-prepared samples were thoroughly rinsed with water and dried with nitrogen before being characterized by electrochemical (EIS) and spectroscopic (IRRAS) techniques.

In the titration experiments, the modified substrate was immersed either in 5 mM KOH or HCl aqueous solutions, and allowed to equilibrate during 20 minutes. Titrations were performed by adjusting the solution pH with a CRISON Basic-20 pH meter upon addition of HCl or KOH. Each pH-equilibrated sample was dried with nitrogen prior to IRRAS characterization. Similarly,

the modified substrate was transferred to the electrochemical cell containing a 1 mM of $K_4Fe(CN)_6$ and $K_3Fe(CN)_6$ in a 0.1 M KNO_3 electrolyte solution, and allowed to equilibrate at the adjusted pH before recording each EIS measurement. At least two freshly prepared SAMs for each surface composition were titrated and characterized by EIS and FT-IRRAS methodologies.

IRRAS and EIS Characterization. A 250 nm thick Au layer adhered to a 2.5 nm thin chromium layer deposited on a 11x11 mm Borosilicate glass were used as (111) textured flat substrates (Gold ArrandeeTM) for the IRRAS measurements. Reflectance-absorption IR spectra were recorded on a JASCO 6300 FTIR single (He-Ne) laser beam spectrometer in the 400-4000 cm^{-1} wavenumbers range at a resolution of 4 cm^{-1}. The data were acquired and further analyzed by the integrated software (Spectra Manager). A variable angle specular reflectance accessory (Pike Technologies-VeeMAX™) assembled in the FTIR spectrometer compartment enabled samples to be analyzed with a p-polarized laser incident beam at a grazing angle of 80º. The reflected IR signal was collected by a MCT-detector. Prior to the measurements, the interferometer and the sample compartments were purged with a dry and free CO_2 air flux of 8 l/min supplied by a compressed air adsorption dryer (K-MT LAB, Parker/Zandet GmbH&Co.KG).

EIS was recorded on an Autolab (Ecochemie model Pgstat 20) instrument attached to a PC with the proper software package (GPES and FRA) for total control of the experiments, data acquisition and analysis. EIS spectra were obtained by applying a sinusoidal excitation signal of 5 mV (AC potential) in a frequency range from 100 kHz to 0.1 Hz to a fixed value (DC potential) corresponding to the standard potential of the ferro/ferricyanide redox probe.

Surface coverage analysis. The relative surface coverage of $–COO^-$ (θ) and –COOH (1-θ) of the SAMs at each pH was determined from the integrated area of the νC=O vibrational bands

corresponding to the IRRAS stretching modes of carboxylate (1400-1445 cm^{-1}) and carboxylic (1700-1750 cm^{-1}) groups. The band area of each individual component was obtained from the best fitting of the experimental data with Gaussian functions assigned to the different vibrational modes of the carboxyl groups by using the non-linear least squares approach. EIS data were fitted to a simplified Randles equivalent circuit allowing to obtain the values of their constituent elements, such as charge transfer resistance, R_{CT}, and double layer capacitance, C_{dl}. R_{CT} values at acidic and alkaline pH were considered representative of the –COOH and –COO- covered surfaces, and their changes related to their surface coverage and acid-base interfacial properties. The titration curves are represented by the averaged values of θ and R_{CT} vs pH of SAMs with different MUA and DT surface compositions (χ_{MUA}^{surf} and χ_{DT}^{surf}). The χ_{MUA}^{surf} was determined from the single peak potential value of the reductive desorption process, E_p^{RD}, obtained in the CV profiles of the pure and mixed SAMs, ~~as described elsewhere~~.[6] The CV profiles and the E_p^{RD} values used match those already reported in our previous work.[6]

Results and Discussion

EIS titration of pure and mixed SAMs of MUA and DT

The ability of SAMs to block the electron transfer (ET) of electroactive species present in solution is a convenient way to evaluate the quality of a monolayer (i.e. compactness and molecular organization) and its interfacial properties. In this sense, EIS provides an appropiate tool to study the ionic permeation and ET barrier properties of pure and mixed organosulphur SAMs on surfaces that allows detecting the presence of defects in the monolayer structure. The presence of defects or pinholes in the SAM enables the redox species in solution to penetrate into the layer at a closer distance or even get in contact with the electrode surface. Then, short-range

ET pathways operate due to the mass transfer of electroactive species through the monolayer to the electrode surface that can compete with the long-range electron tunnelling mechanism. [6, 25, 26] Consequently, an increase of the heterogeneous rate constant, k_{ET}, of the redox reaction is usually associated with a decrease of the apparent thickness of the insulating layer due to a lower degree of structural integrity of the SAM.

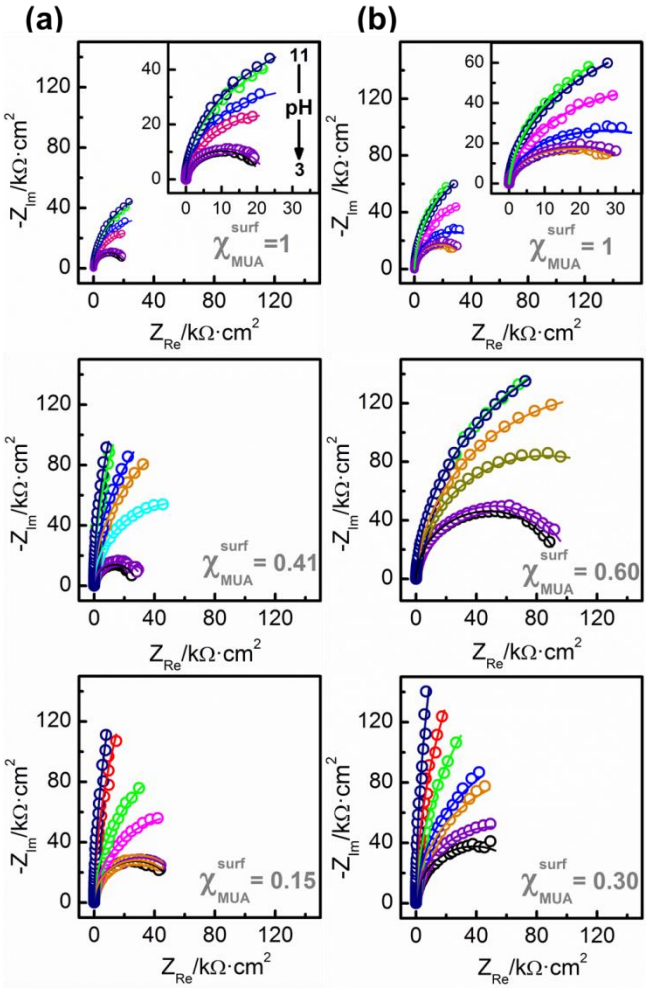

Figure 1. Nyquist plots of SAMs formed from a micellar medium at (a) 15 min and (b) 18 h of modification time and different MUA surface compositions, χ^{surf}_{MUA}, recorded in a 1mM $K_4Fe(CN)_6/K_3Fe(CN)_6$ + 0.1 M KNO_3 solution as a function of the pH: 3 (●), 5 (●), 6 (●), 6.5

(○), 7 (○), 7.5 (○), 8 (○), 8.5 (○), 9 (○), 10 (○) and 11 (○). $E_{1/2}$ = 0.17 V vs SCE. The solid lines are the fits of experimental data to the simplified Randles equivalent circuit ($R_u[CR_{ct}]$).

Figure 1 shows the EIS response (*Nyquist plots*) of $Fe(CN)_6^{3-/4-}$ on Au surfaces modified with pure and mixed MUA/DT SAMs, at different modification times and surface compositions as a function of the solution pH. The impedance spectra profiles show a typical semicircular shape at the entire range of frequencies. The absence of a straight line at low frequencies indicates that the contribution of diffusion-controlled mass transfer processes to the total faradic impedance can be neglected. This fact agrees with a good blocking behavior of the SAMs towards the redox probe reaction at the gold surface. The best fitting of EIS data was obtained by using a simplified Randles equivalent circuit consisting of a parallel combination of a capacitor, C, and charge transfer resistance, R_{CT}, in series with the uncompensated solution resistance, R_u (Figure 1). The diameter of the semicircle in the EIS curves defines the R_{CT} value, which is inversely proportional to k_{ET}. [6, 26] ~~Figure 1 shows that the impedance is approximately two fold for the layers built at the largests modification time~~. Figure 1 shows that the Nyquist plots corresponding to the layers built at the largest modification time achieve higher impedance values than those obtained at the shortest with roughly similar surface compositions. This is due to the improvement in the ET blocking properties of the SAMs formed at near-to-equilibrium conditions and whose structures possess a smaller number of defects and better mixing of their constituents at the molecular scale.[6]

It is also worth noting that the diameter of the semicircle gets larger while increasing the solution pH independently of the modification time and surface composition of the SAMs. Therefore, changes in the R_{CT} values with pH must be directly related to the influence of the ionization of the -COOH groups at the SAM/electrolyte interface on the kinetics of the ET

reaction of the $Fe(CN)_6^{3-/4-}$ redox probe.[27-30] The improvement in the ET blocking behavior of the interface at higher pHs can be interpreted by the higher charge density of the SAMs when their surface content of dissociated -COOH head groups increases. The reason is that the more negatively charged the SAM interface is, the greater surface potential difference between the outer plane of closest approach (OHP) and the bulk solution, Φ_1. Under these conditions, the negatively charged redox probes are prevented from approaching the surface due to electrostatic repulsion, which in turns causes the depletion of the $Fe(CN)_6^{3-/4-}$ surface concentration at the OHP zone in the electrical double layer.[31-33] Then, in the presence of double layer effects, R_{CT} can be expressed as: [32, 34]

$$R_{CT} = R_{CT}^{0} \cdot e^{\left[(z-\beta n)\frac{-F\Phi_1}{RT}\right]} \qquad (1)$$

where z is the charge of the redox probe, $\beta=1-\alpha$, with α the electron transfer coefficient, and R_{CT}^{0} is the charge transfer resistance value for $\Phi_1=0$ (i.e. uncharged monolayer). Similarly, the interfacial capacitance in the double layer, C, should be influenced by the dielectric properties of the SAM and its acid-base surface properties. Therefore, it is reasonable to assume that C would reflect changes in the surface composition of the mixed SAMs and in the degree of dissociation of the ω–carboxylic head groups.[34-37]

The C and R_{CT} values of the titrated SAMs determined from EIS analysis are plotted in Figures 2 and 3, respectively. Although the interfacial capacitances depend on the SAMs surface composition, their values are hardly influenced by the changes in pH. This has been also reported by Kakiuchi et al.,[36] where capacitance titration curves of ionizable SAMs were only applicable to those with shorter chain lengths (HS-(CH_2)n-COOH with $n < 10$). Thus, assuming that the degree of dissociation of the end-groups does not significantly contributes to the measured

capacitance, we can average the values at every surface composition and relate them to the mole fraction of both components within the SAM.

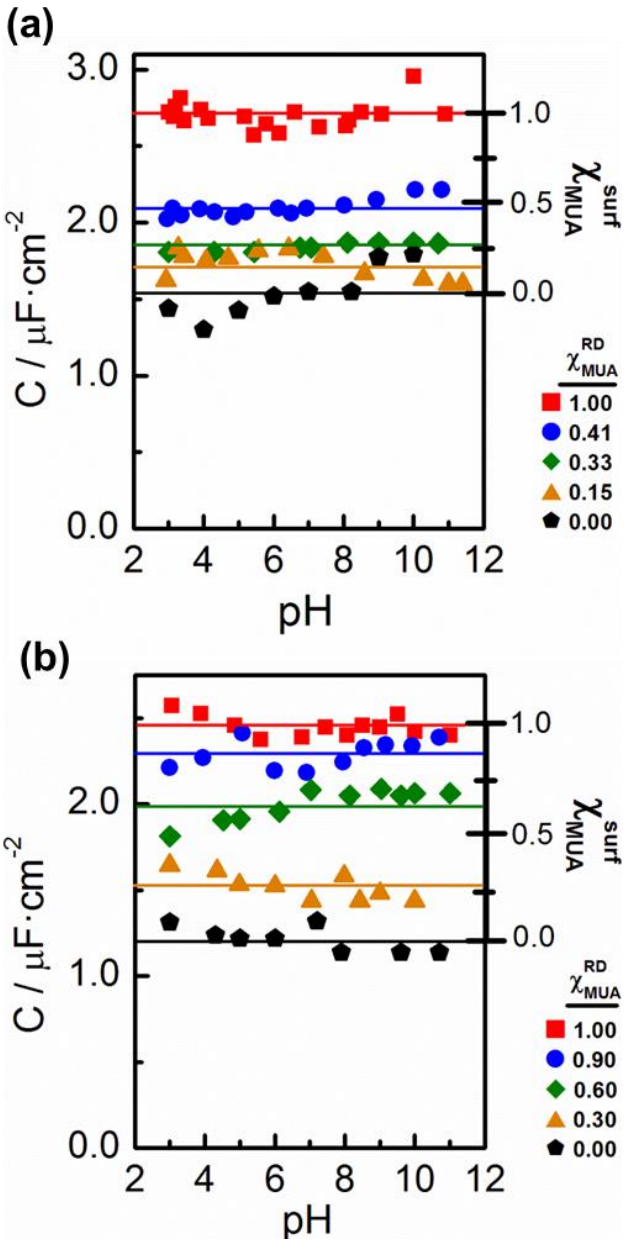

Figure 2. Capacitance titration curves for pure and mixed SAMs of MUA and DT formed at a) 15min and b) 18h. The solid lines represent the average capacitance at the different surface compositions. The MUA surface composition of the SAMs, χ_{MUA}^{RD}, is determined from the

voltammetric ~~peaks~~ peak of their reductive desorption process and depicted in the figure legends.[6] The right axis show the MUA surface compositions, χ_{MUA}^{surf}, calculated by using eqn. (2).

The capacitance at a SAM/electrolyte interface, C, can be viewed as a series combination of C_m^{SAM} (monolayer) and C_{dl} (double layer). In general, C_m^{SAM} of long chain alkanethiol layers is at least one order of magnitude smaller than C_{dl} in electrolytes of ~0.1 M concentration that makes $C \sim C_m^{SAM}$. [38] From a macroscopic perspective, C_m^{SAM} of a mixed monolayer will consist of the sum of the capacitance value of the pure SAMs of each component, C_m^{MUA} and C_m^{DT}, weighted by their mole surface fractions. [37] Then, the surface composition of the mixed SAMs can be calculated by using the following expression:

$$\chi_{MUA}^{surf} = \frac{C - C_m^{DT}}{C_m^{MUA} - C_m^{DT}} \qquad (2)$$

The values of χ_{MUA}^{surf} determined from equation (2) are in reasonable agreement with those obtained by the method based on the use of the reductive desorption potential of the SAMs.[6] The underlying limitations of this indirect method are similar to others and, in this particular case, to the assumption that the "effective thickness" of the layers is equivalent to their dielectric thickness and remains constant with changes in the mixed SAM composition. Additionally, these low capacitance values would indicate the presence of well-organized and compact SAMs. This kind of SAMs behaves as an ideal dielectric layer modeled by a simple double layer capacitor:

$$C = \frac{A}{d} \varepsilon_o \cdot \varepsilon_m \qquad (3)$$

where C is the SAM capacitance, A the surface area, d the layer thickness, ε_o the permittivity of free space, and ε_m the relative permittivity of the layer.

Then, the relative permittivity determined for the pure SAMs can be taken as an average of the film quality. The thickness of MUA and DT SAMs is 12.5 and 11.2 Å, respectively, assuming

that the molecules are organized into a well-packed structure with their hydrocarbon chains in an all-trans configuration and a tilt angle of 30°.[39] The ε_m values determined by using the eqn. (3) range between 1.6-2.0 and 3.5-3.8 for pure SAMs of DT and MUA, respectively. In the case of DT layers, such values agree with those reported in the literature for the dielectric constant of polyethylene and well-ordered alkanethiol SAMs.[40-42] The value of ε_m for the MUA SAMs is also consistent with the higher polar character of well-packed ω-terminated SAMs (e.g. ε_m = 3, 4 and 3.5-6.6 for –OH, –SH and –COOH as terminal groups, respectively).[36, 42-44] These results confirm that the SAMs behave as a dielectric medium of approximately the expected thickness, and in turn this methodology is appropriate to determine the surface mole fraction of their components.

Figure 3 shows that R_{CT} clearly changes with pH for each SAM composition in contrast to what happens with the interfacial capacitance, C. Such changes are addressed by the dependence of the potential at the double layer, Φ_1, on the level of ionization of the –COOH groups of the monolayer, θ, as a function of the solution pH (Eqn. (1)). For an interfacial acid-base reaction at equilibrium, the degree of dissociation of surface immobilized –COOH groups is expressed as: [35]

$$\log \frac{\theta_{surf}^{COO^-}}{\theta_{surf}^{COOH}} = \log \frac{\theta}{1-\theta} = pH - pK_a + \frac{F\Phi_2}{2.303RT} = pH - pK_{1/2}^{app} \quad (4)$$

where Φ_2 is the potential at the Helmholtz plane of acid dissociation (PAD) of the monolayer referred to the potential in the bulk solution, K_a is the dissociation constant of the surface bound acid group in the absence of interfacial electric fields (Φ_2=0), and $pK_{1/2}^{app}$ is the pH when half of the groups are ionized (θ=0.5). Thus, $pK_{1/2}^{app}$ includes the contribution to the shift of pK_a caused by electrostatic and intermolecular interactions in the SAM/solution interface. Assuming that $Fe(CN)_6^{3-/4-}$ do not adsorb specifically at the SAMs interface, Φ_1 may be identified with Φ_2, and then equations (1) and (4) appear directly related.

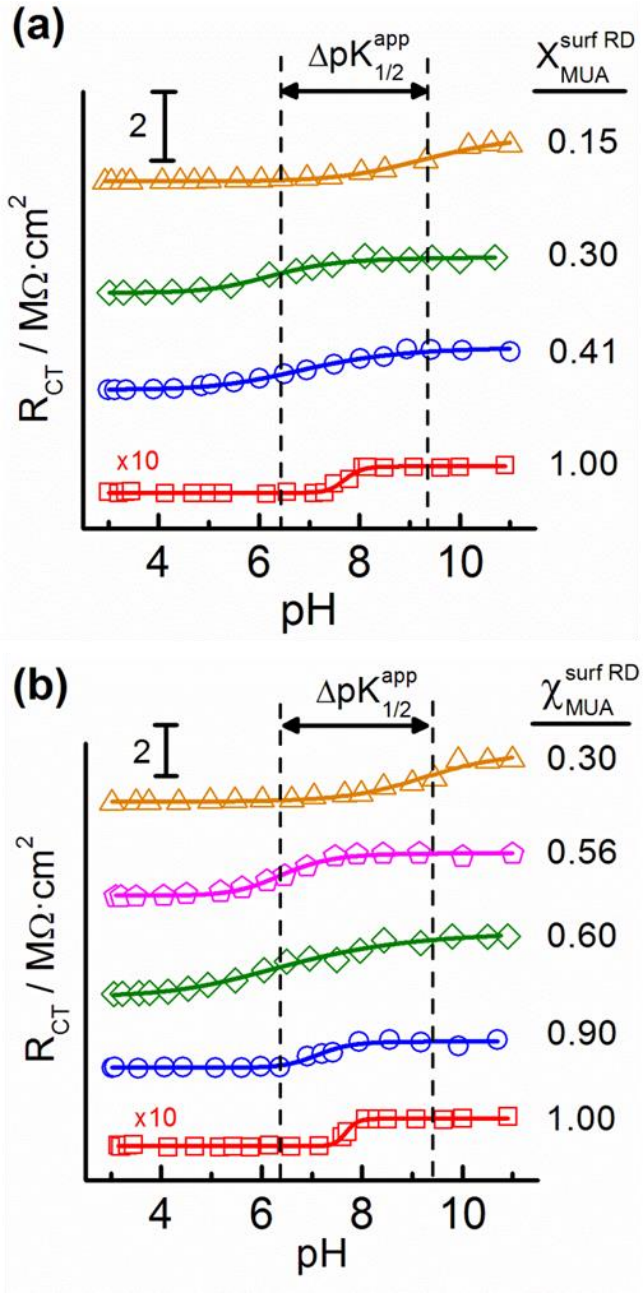

Figure 3. Charge transfer resistance titration curves of pure and mixed SAMs of MUA and DT formed at a) 15min and b) 18h from a lyotropic medium with different surface compositions.

Therefore, the titration curves shown in Figure 3 relate to the changes of θ for pure MUA and mixed SAMs. Under acidic conditions, R_{CT} remains constant, which is characteristic of SAMs

with interfacial charge densities that keep pH-independent because their –COOH terminal groups remain fully protonated and uncharged (i.e. R_{CT}^{0} in equation (1)). Under basic conditions, R_{CT} increases to attain a limiting value representative of SAMs almost fully deprotonated with higher charge densities. At intermediate pH values, there is a transition region from low to high R_{CT} values which extends over several pH units while θ is increasing. The spreading of the titration curves depends on the electrostatic interactions between neighboring charged groups. The pH at the steepest slope of the curves is taken as the apparent surface pK_a value of the SAMs ($pK_{1/2}^{app}$). All EIS titration curves show a single $pK_{1/2}^{app}$ for the acid-base equilibrium reaction at the SAM interface and their values are depicted in the Table 1.

Table 1. Apparent pK values of pure MUA and mixed SAMs obtained from EIS and IR data.

χ^{surf} MUA/DT	$pK_{1/2}^{app}$ EIS titration		$pK_{1/2}^{app}$ IR titration	
	15 min	18 h	15 min	18 h
1.00/0.00	7.7	~~8.3~~ 7.8	7.5	7.7
0.90/0.10	-	7.1	6.9	7.2
0.60/0.40	-	6.7	-	9.1
0.41/0.59	7.0	-	4.0/7.3	-
0.30/0.70	6.3	9.2	-	9.4
0.15/0.85	9.4	-	4.5/9.7	-

The standard deviations for the $pK_{1/2}^{app}$ values are lower than 12 % in all cases

In order to explain the spreading of the titration curves and the variation of $pK_{1/2}^{app}$ values with the surface composition of the SAMs, the variation of Φ_2 with θ needs to be considered.

According to the 1-pK model, the potential is related to the energy of electrostatic interactions of charged molecules with its surroundings, $\Phi_2 = -\overline{E}\theta / F$. Moreover, the extension of the statistical mechanical model developed by Borkovec et. al. to ionisable solid-liquid interfaces allows the following expression to be applied to the titration curves: [45]

$$\log \frac{\theta}{1-\theta} = pH - pK_a - \frac{\overline{E}\theta}{2.303RT} = pH - pK_a - \frac{\beta\overline{E}\theta}{2.303} \qquad (5)$$

When the interaction parameter, $\beta\overline{E}$, increases the titration curves broaden and their inflection midpoint shifts to higher values by $pK_{1/2}^{app} - pK_a = \beta\overline{E}\theta/2.303$ with $\Delta pK_{1/2}^{app} = \beta\overline{E}/2.303$. In the absence of electrostatic interactions ($\beta\overline{E} = 0$), eqn. (5) coincides with that for the acid-base equilibrium of free carboxylic acids in the bulk solution. Figure 3 shows that EIS titration curves extend over several pH units with their $pK_{1/2}^{app}$ shifted to pH values higher than that of alkanoic acids in solution (pK_a~4.5). This behavior may be invoked by the electrostatic interactions between neighboring ionized groups that are less efficiently screened in well-organized SAMs. Thus, the proton concentration at the Helmholtz PAD region becomes larger than that in the bulk solution and the dissociation of the terminal groups gets more difficult as θ increases due to the restricted access of the –COOH moieties and the reduced solvation of the interfacial $–COO^-$ groups. As a result, when the intermolecular and electrostatic interactions increase (i.e. $\beta\overline{E}$), the displacement of $pK_{1/2}^{app}$ to basic pHs and its spreading before ionization is completed are larger.

The 1-pK interaction model based on the continuous charge at the double layer is well-reproduced by the titration curves presented here. Table 2 shows the values of K_a and $\beta\overline{E}$ that have been estimated from the best fits of the equation (5) to the experimental data. The $pK_{1/2}^{app}$ values determined for MUA layers formed at low and high modification times are 7.7 and ~~8.3~~

7.8, respectively (Table 1). When an interaction parameter of $\beta\bar{E}/2.303 = 1$ is considered, intrinsic pK_a values of 7.2 and 7.3 are obtained (Table 2). These results are within the range of values reported in literature for the pK_a of carboxyl-terminated SAMs determined by EIS [21, 27-29, 32] and FTIR [46-49] titration experiments, which are comprised between 5.3 and 8. In the electrochemical titration experiments, the pK_a of the SAMs can be influenced by the applied external potential that additionally alters the interfacial surface charge. Thus, at more negative potentials than that of the zero charge of the SAM, E_{pzc}, the electrostatic repulsion between the negatively charged metal surface and the $-COO^-$ groups at the PAD region is reduced by favoring protonation, and thus the $pK_{1/2}^{app}$ must increase. This effect is shown by Sanders et. al. [28] in the EIS titration of MUA SAMs using $Fe(CN_6)^{3-/4-}$ or $Ru(NH_3)_6^{3+/2+}$ redox probes with their standard potentials, $E_{1/2}$, more positive and negative than the E_{pzc} of the monolayer, respectively. The surface pK_a was stablished around 6, somewhere between the $pK_{1/2}^{app}$ values obtained from every redox probe. In general, the pK_a values range between 5.3 and 6 for carboxyl-terminated monolayers deposited from ethanol that are electrochemically titrated by using $Fe(CN)_6^{3-/4-}$. [21, 27-29, 32, 50] The higher $pK_{1/2}^{app}$ values found here for the MUA SAMs formed from a micellar medium may be partially related to favored intermolecular interactions due to a better organization and compactness.[51, 52] However, the $pK_{1/2}^{app}$ and intrinsic pK_a values are still about 3-4 units higher than that of alkanoic acids in solution which cannot be easily accounted only by repulsive interactions as the 1-pK model predicts. Therefore, the additional contribution of electrode potential,[28, 49] hydrogen bonding, [36, 53] ion solvation and hydrophobic [35, 36, 48, 49, 54, 55] effects must be also present in the vicinity of the SAM PAD layer.

Table 2. Intrinsic pK and interaction parameter values of the SAMs determined from eqn. (5).

χ^{surf} MUA/DT	EIS titration				IR titration			
	15 min		18 h		15 min[(a)]		18 h	
	pK_a	$\frac{\beta\bar{E}}{2.303}$	pK_a	$\frac{\beta\bar{E}}{2.303}$	pK_a	$\frac{\beta\bar{E}}{2.303}$	pK_a	$\frac{\beta\bar{E}}{2.303}$
1.00/0.00	7.2	1	7.3	1	6.2	3	6.2	3
0.90/0.10	-	-	6.4	1-2	5.9	3	6.4	3
0.60/0.40	-	-	4.7	5	-	-	7.2	3
0.56/0.44	-	-	5.5	2	-	-	-	-
0.41/0.59	5.9	2	-	-	5.7	3	-	-
0.30/0.70	5.6	2	7.6	3	-	-	7.2	3
0.15/0.85	8.1	2	-	-	7.7	3	-	-

(a) The interaction parameters depicted only correspond to the higher pK_a value.

Noteworthy, the acid/base properties of the SAMs are altered when the MUA surface composition, χ^{surf}_{MUA}, varies. This is shown in Figure 3 by the changes in the spreading of the EIS titration curves and the $pK^{app}_{1/2}$ values of the MUA/DT mixed SAMs which display a similar behavior independently of the time employed for its formation. It is observed that the dilution of the –COOH groups by DT molecules initially provokes the $pK^{app}_{1/2}$ and the intrinsic pK_a to progressively decrease up to approximately 1.5 ~~2.5~~2.0 pH units, respectively (Tables 1 and 2). This increase of the SAMs´ acidity is consistent with the predominant effect of the lowering of in-plane repulsive interactions between charged groups compared to hydrophobic effects due to the lowering of the local dielectric constant, ε_S, by the insertion of $–CH_3$ terminal groups.[36, 54] Such behavior is resembled by well-ordered and homogeneously patterned SAMs (i.e. non-

segregated) with –COOH chains that are molecularly or nanoscopically distributed into 2D arrays of alkyl chains with similar length, as it might be the present case.[48, 55] Otherwise, if the alkyl and carboxylic chains were segregated into microscopic domains the spreading of the titration curves and the $pK_{1/2}^{app}$ of the SAMs would be expected to be independent of the dilution of the ionizable groups as their local environment would be hardly affected at the domain boundaries. [48]

Nevertheless, the opposite shift in the surface pK_a has been also described in short-chain [27, 54] and long-chain [54] COOH-terminated SAMs mixed with alkanethiols of similar length. The spare adsorption [26] and the greater disorder [54] of the –COOH terminated molecules at short-chain mixed SAMs was argued to increase the groups´ basicity because of their embedment in a local environment where ion solvation and hydrophobic effects predominates. In the case of long-chain SAMs (n>10), the $pK_{1/2}^{app}$ rises while increasing the alkyl chain length of the diluent $–CH_3$ groups (n = 9-12) which was related to a progressively less polar environment surrounding the –COOH sites. Thus, a low local dielectric constant would disfavor ionization of the polar groups due to their poorer electrostatic solvation and stabilization by the counterions. [27, 35, 49, 54, 55]

The influence of SAM ordering and the relative difference in the backbone length between the –COOH and $–CH_3$ molecules would help to reconcile both behaviors. Thus, –COOH terminated SAMs homogeneously mixed with alkanethiols of similar or longer chain length and/or with some degree of structural disorder which buries the polar groups may show the predominant effect of the hydrophobic environment in its vicinity. On the other hand, well-ordered and homogenously mixed SAMs composed of shorter alkanethiol molecules with the $–CH_3$ groups embedded underneath the –COOH moieties may reflect a predominant effect of the lowering of

in-plane repulsive interactions. It has been also inferred that the ionization of the –COOH groups appears to be unaffected when the chain length of the alkanethiols is similar or shorter only by 2 and 4 methylene units.[48] However, this would be contradictory for a homogeneous distribution of –COOH and $–CH_3$ groups with all of them being accessible by water molecules, and where $–COO^-$ solvation should be still affected by the local hydrophobicity created by $–CH_3$ groups closely placed underneath. [48, 56] Then, the following question comes out: why the lowering of repulsive interactions could arise in homogeneously mixed SAMs of MUA and DT with similar chain length? A possible answer would be that hydrophobic interactions might be shielded by the rearrangement of the acid groups lying on top the neighboring $–CH_3$ terminated chains.[48]

Interestingly, when the χ_{MUA}^{surf} is further decreased, the $pK_{1/2}^{app}$ and the intrinsic pK_a values of the SAMs display a large shift of approximately 2-3 pH units but now in the opposite direction (Tables 1 and 2). The trend of the $pK_{1/2}^{app}$ to decrease is then reversed to increase the surface groups´s basicity, with such a change taking place at a lower surface content of DT for the SAMs built at the higher time (Figure 3). This could be feasibly interpreted in the terms of the different spatial distribution of DT and MUA molecules into these homogeneously mixed SAMs.[6] If the –COOH and $–CH_3$ groups would be ideally mixed at the molecular level, the electrostatic interactions in well-ordered SAMs should decrease to a minimum for a 1:1 surface composition of both components compared to that of the pure MUA SAM. Thereafter, the dilution of the –COOH groups beyond $\chi_{MUA}^{surf} < 0.5$ would provoke a gradual increase of the local hydrophobicity due to the excess of neighboring $–CH_3$ groups that cannot be all shielded anymore by polar moieties placed on top. This scenario is more closely resembled by the MUA/DT mixed SAMs built at the higher modification time that already show an increase on the $pK_{1/2}^{app}$ at $\chi_{MUA}^{surf} \sim 0.3$. In

the case of the less homogeneously mixed SAMs built at the shorter time, such effect does not become evident until an excess high enough of $-CH_3$ groups is probably surrounding the MUA nanodomains ($\chi^{surf}_{MUA} \sim 0.15$).[6] In this framework of polar groups highly diluted, both molecular mixing and few MUA molecules ~~segregated~~ arranged in small domains may converge into a less discernable scenario of quite similar local hydrophobic environments. A similar conclusion could be drawn if the binary SAMs become sparsely adsorbed and structurally disordered. [27, 49, 54] In fact, the MUA/DT SAMs formed at the lower modification time are prone to disorder when $\chi^{surf}_{MUA} < 0.3$. [6] These results suggest that the interfacial acid-base properties of binary SAMs are modulated by the degree of homogeneity in the distribution of their constituents at the molecular scale leading to different surface patterns.

IRRAS titration of pure and mixed SAMs of MUA and DT

Figure 4 shows the IR spectra at the low wavenumbers region (1300-1800 cm^{-1}) of MUA monolayers deposited on an Au(111)-textured surface which are exposed to basic and acid aqueous solutions. The vibrations of the -C=O groups are clearly identified at the IR spectra by the appearance of five characteristic adsorption bands.[57] Those centered at 1740 (ν_{nb}) and 1715 cm^{-1} (ν_b) are assigned to the –C=O stretching modes associated with non-hydrogen and hydrogen bonding interactions, respectively.[58, 59] The relative intensities of these peaks has been recently reported as a way to evaluate the quality of the SAMs due to its sensitiveness to the surface flatness and nanotopology of the Au(111) substrates.[60] In the case of Au(111) single crystals with low miscut angles (<0.1°) and large atomically flat smooth terraces (>100 nm), the SAMs´ uniformity is greatly improved by favoring intermolecular interactions. As a consequence, only the peak associated to hydrogen bonded groups appears. [60] However, in Au(111)-textured

surfaces gathering many grains, both peaks at 1740 and 1715 cm^{-1} are present due to structural defects induced in the SAM by step edges and grain boundaries at the surface topography.[47, 60] This fact affects the acid-base behavior of the carboxylic SAMs in the way that the electrostatic repulsion between terminal groups is higher at atomically flat gold surfaces. [47, 60] The vibrational band at 1468 cm^{-1} is attributed to the scissors deformation mode of the $–CH_2$ groups (δ_{sc}-CH_2) in the alkyl chain. The remaining bands are ascribed to the asymmetric, ν_{as} (1440 cm^{-1}) and symmetric, ν_s (1410-1420 cm^{-1}) stretching modes of the carboxylate groups.[47, 60, 61]

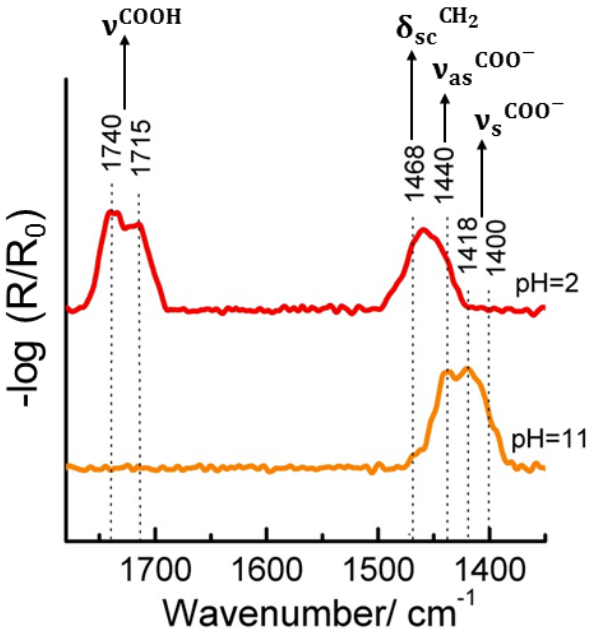

Figure 4. Typical IRRA spectra in the low frequency region of a MUA monolayer deposited on Au(111)-textured from a lyotropic medium and immersed in alkaline and acid aqueous solutions.

Figure 5 shows the IR spectra of pure MUA and mixed MUA/DT monolayers formed at different modification times that are titrated in the pH range of 2 to 11. As expected, the intensity of the vibrational bands belonging to the -COOH and $–COO^-$ groups is clearly pH-dependent. When the pH decreases to ~4-5, the bands associated to the $–COO^-$ groups diminish while the

band assigned to non-hydrogen bonded –COOH groups, ν_{nb}, and that of the δ_{sc}-CH_2 mode concomitantly increase during the protonation of the MUA molecules. When the pH is further decreased, the general trend observed is that the δ_{sc}-CH_2 band now decreases while the band associated to hydrogen bonded -COOH groups, ν_b, concomitantly appears and increases. Finally, a small fraction of non-titrated $–COO^-$ groups is still present on the surface even at very low pHs. These observations would be compatible with different structural rearrangements and tilted orientations of the backbone and the –COOH terminal groups of the SAMs during their titration.

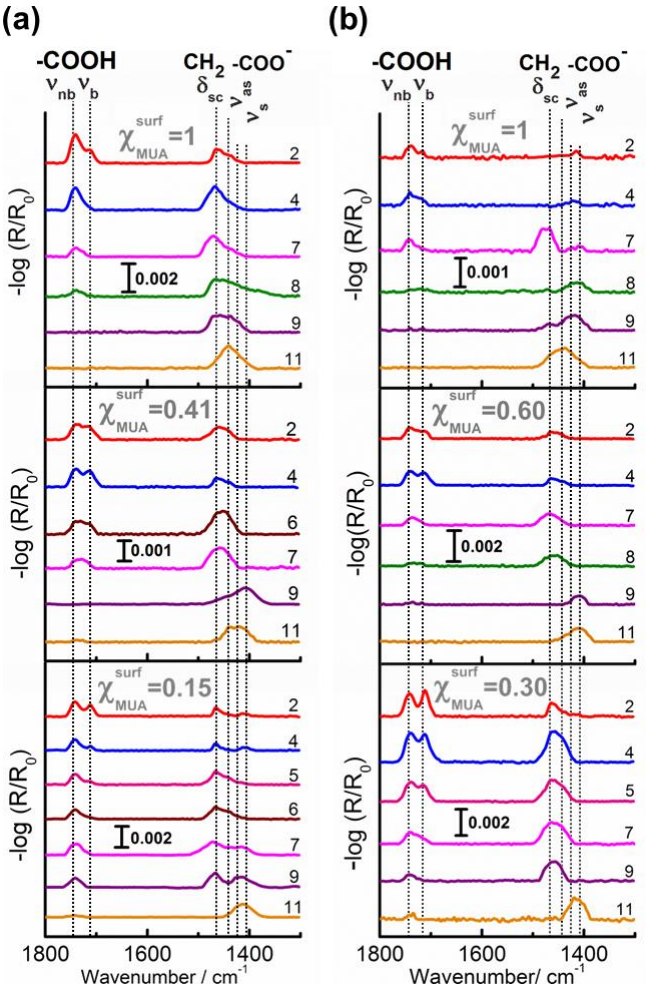

Figure 5. IR titration spectra of pure and mixed MUA/DT SAMs on Au(111) formed from a lyotropic medium after (a) 15 min and (b) 18 h of modification time. pH values are labeled in the right hand side of each IRRAS spectrum.

In an attempt to unravel this assumption, IRRA spectra of the SAMs were analysed in the high wavenumbers region where the characteristic bands of the symmetric, d^+, and asymmetric, d^-, stretching modes of the $-CH_2$ groups at the hydrocarbon chain appear. The peak position and width of these vibrational modes are sensitive to the conformational order of the SAMs. A crystalline structure with the alkyl chains mainly in all-trans conformation is associated with d^+ and d^- bands positioned at 2849-2850 and 2818-2819 cm^{-1}, respectively. [40, 58, 62, 63] The bands broaden and shift to higher wavenumbers when the conformational order of the alkyl chains progressively decreases and the SAM structure becomes increasingly disordered. [40, 58, 62, 63] Figure 6 shows that the MUA/DT mixed SAMs equilibrated at pH 11 exhibits a crystalline-like conformational order except those built at 15 minutes with $\chi_{MUA}^{surf} < 0.41$ which are disordered as their d^+ and d^- bands appear displaced to 2853 and 2924 cm^{-1}, respectively. These results agree with that reported for these mixed SAMs at pH 7.[6] During the acidic titration of the SAMs, the d^+ and d^- bands broaden and displace their position to higher wavenumbers while their intensity increases due to changes in the transition dipole moment projection of the C-H stretching vibrations along the surface normal direction (Figure 6a). Such changes are attributed to the rearrangement of the alkyl chains by the protonation of the terminal groups, and consequently to configurations that are different from the canted orientations at crystalline-like SAMs.[63] On the other hand, the SAMs with lower conformational order and gauche defects in its structure showed only an increase in the intensity of the bands without any displacement in their position (Figure 6b). Although the structure of these SAMs may also be altered by the acid/base interfacial reactions they remain in a disordered state. Such structural rearrangements and the gradual disordering of the SAMs would justify the changes in intensity of the δ_{sc}-CH_2 band and that a small fraction of $-COO^-$ groups were not protonated due to its burying even at low pHs.

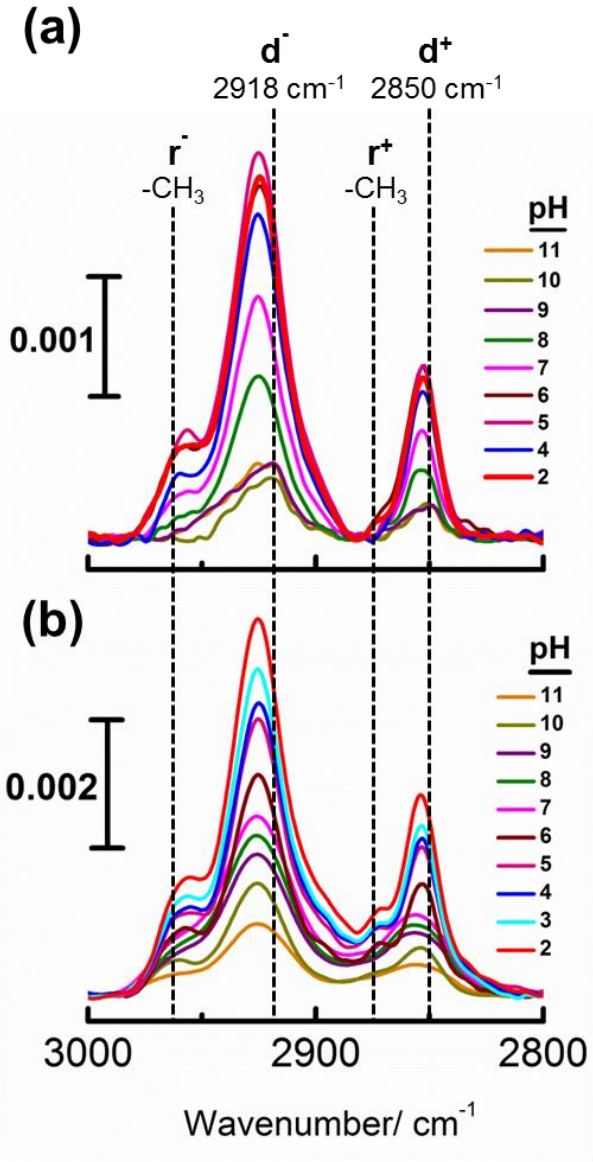

Figure 6. Representative behavior of the evolution of the position and intensity of the d^- and d^+ IR bands during the acidic titration of mixed MUA/DT SAMs formed at: a) 18 h for all χ_{MUA}^{surf} compositions and 15 min for $\chi_{MUA}^{surf} > 0.41$, and b) 15 min for $\chi_{MUA}^{surf} = 0.41$ and 0.15.

The surface ratio of –COOH/-COO^- in the SAMs can be determined at each pH from the integrated peak area of their IR bands assuming that the extinction coefficients vary similarly. Figure 7 illustrates the changes in the degree of dissociation of the –COOH groups, θ, with pH

for SAMs formed at different times and surface compositions. The IR titration curves are well fitted by the 1-pK model and the acid-base behaviour of these assemblies agrees with that commented above by electrochemical means. Thus, the dilution of MUA also initially decreases the $pK_{1/2}^{app}$ and intrinsic pK_a of the SAMs by reducing their electrostatic interactions, and finally to turn over again to the opposite trend by the predominance of local hydrophobicity (Tables 1 and 2), what is also extended to lower χ_{MUA}^{surf} values in the SAMs formed at 15 minutes. This reinforces the drawn idea based on the influence of the surface patterning at homogeneously mixed SAMs compatible with the rearrangement of -COOH groups on top of the $–CH_3$ chains of similar length that may play a role in the restructuration of their backbones during titration.

Nevertheless, IR titration curves put forward some additional aspects to consider. Figure 7a shows that the mixed SAMs formed at 15 minutes have a more complex interfacial behavior with two different $pK_{1/2}^{app}$ emerging at low surface coverages of MUA. Such a difference with EIS titration behaviour providing a single pK may be a consequence of the way IRRAS experiments interrogates the interface in the absence of an external potential and a redox probe as mediator. There are only a few examples reported in literature of SAMs, either with one or two surface-confined ionizable groups, showing two discernible pK_a. [46, 53, 64] Gershevitz et al.[46] firstly addressed two pKs in carboxyl-terminated alkylsiloxane monolayers anchored on Si. The first pK_a (~4.9) was assigned to –COOH monomers and the second one (~9.3) to dimeric and oligomeric species whose association was related to changes in the alkyl chain conformation and groups acidity. Other authors have found that the formation of strong ionic hydrogen bonds (i.e. $–COOH\cdots {}^{-}OOC-$) leads to higher pK_a values (~8.4). [53, 65] Such interaction is promoted under low ionic strength and reduced local dielectric constant (ε~1) conditions, where association of $–COO^-$ with cations is unfavourable and the water is expelled from the interaction volume.[53, 65, 66]

Nuzzo et al.[58] argued that SAMs of mercaptohexadecanoic acid (MHDA) on Au were composed only by a small fraction of hydrogen bonded groups forming linear oligomers instead of head-to-head dimers. On the other hand, the existence of head-to-head dimers is also addressed by FTIR (ν_bC=O at 1715 cm^{-1}) in MHDA and MUA monolayers whose structure is slightly distorted.

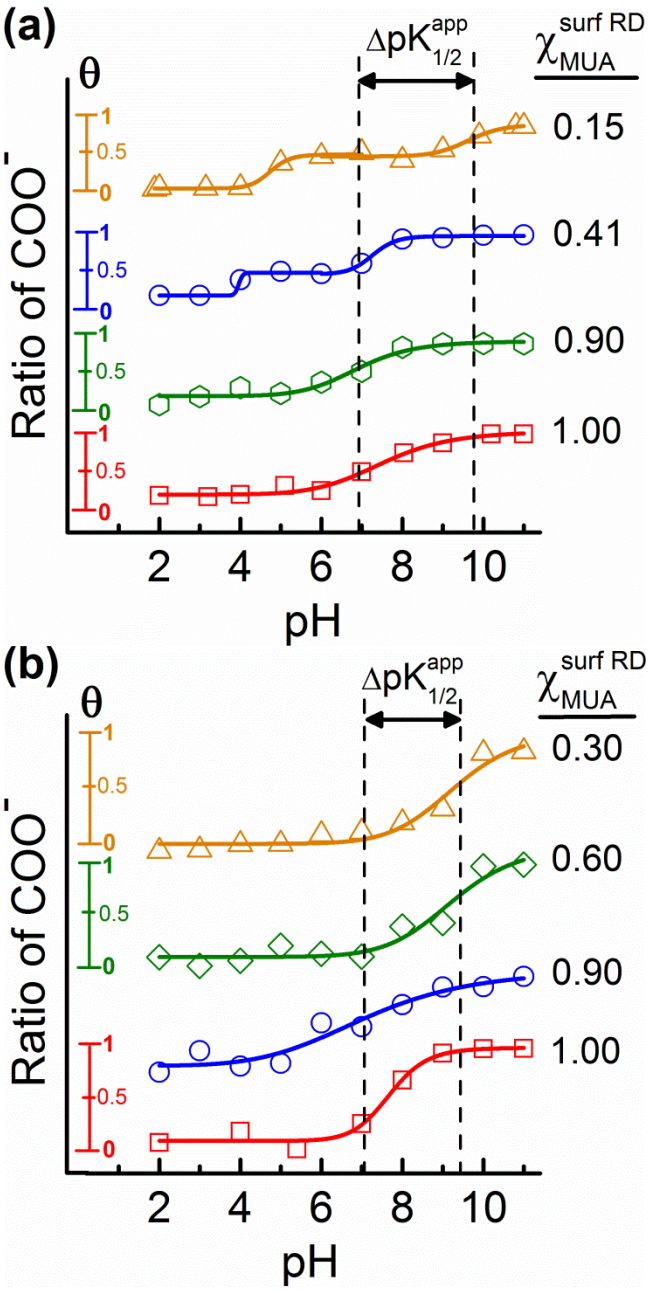

Figure 7. IR titration curves obtained by plotting the surface coverage of $-COO^-$ groups, θ, vs pH for monolayers of MUA and DT formed from lyotropic medium at: a) 15min and b) 18h, with different surface compositions (χ^{surf}_{MUA}).

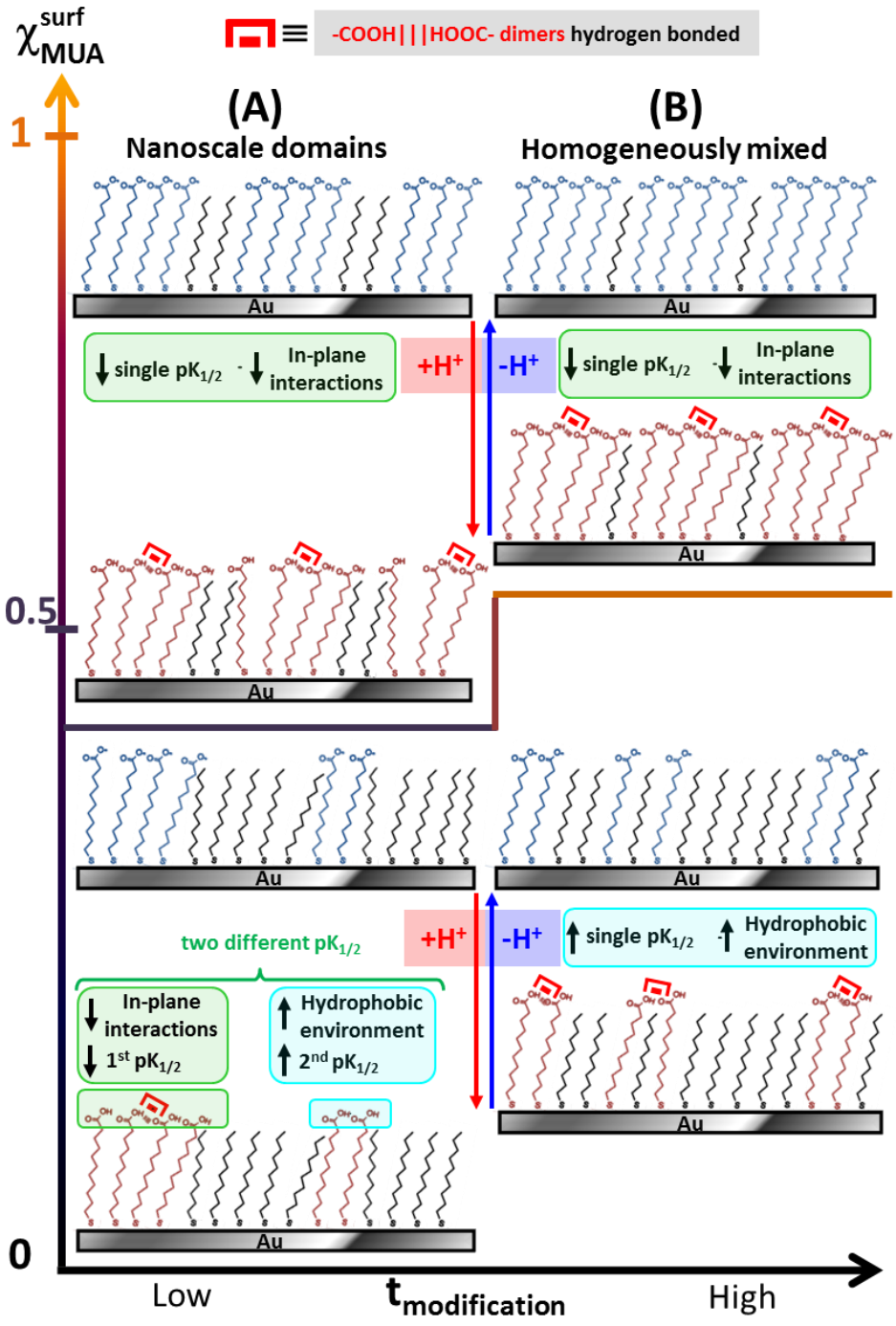

Scheme 1. Acid/base interfacial properties of homogeneously mixed MUA/DT SAMs vs surface composition: (A) nanodomains and (B) molecularly distributed components.

In this sense, the first scenario proposed to explain the present results is based on the surface distribution of MUA molecules into nanodomains of different size (Scheme 1). At $\chi_{MUA}^{surf} > 0.41$, the average size of the MUA domains may be still large enough for the $-COO^-$ groups to be mainly protonated in quite similar local environments as it would happen to a pure MUA SAM, but with their repulsive interactions reduced by the diluting effect of homogenously mixed DT molecules that allow the $pK_{1/2}^{app}$ to slightly decrease (Tables 1 and 2). Similarly to what happens in pure MUA SAMs (Figure 5a), the –COOH groups rearrange and some structural disorder is induced in the alkyl chains during this single protonation step. When $pH << pK_{1/2}^{app}$, an additional rearrangement of the alkyl chains and the –COOH groups takes place in the already distorted structure of these SAMs, which probably provokes the formation of hydrogen bonded dimeric species inside the domains as demonstrated by the evolution of both δ_{sc}-CH_2 and ν_bC=O bands.

At $\chi_{MUA}^{surf} < 0.41$, the emergence of two protonation steps is associated to two different local environments that alter the acidity of the ionisable groups. Figure 7a shows that each molecular environment represents approximately half of the total surface coverage of MUA. In order to explain such behaviour, it is assumed that the MUA molecules are mainly divided in two different arrangements composed by nanodomains of smaller and larger size (Scheme 1A). The distribution of the MUA molecules into isolated entities or in small groups would imply closer to ideal thermodynamic conditions of homogenous mixing at the surface. The smallest "domain" size would be ideally composed only by one or two $-COO^-$ groups as isolated monomers or dimers. The MUA molecules associated in the smallest numbers and/or in larger groups but located at the domain boundaries would be firstly titrated among the overall at the higher $pK_{1/2}^{app}$

value due to their lowest local dielectric environment. This effect can be favoured because of these mixed SAMs are originally disordered and some of the –COOH moieties might be also buried in the hydrocarbon scaffold. In a next step, the $–COO^-$ located mainly inside of sufficiently large MUA domains would be subsequently protonated at the lower $pK_{1/2}^{app}$ value (~4 to 4.5). Such values are quite similar to that of the carboxylic acids in bulk solution and in agreement with the loss of efficient intermolecular interactions in structurally disordered assemblies. The –COOH groups would be able to rearrange and link together to form hydrogen bonded dimeric species in both kind of environments as it is demonstrated by the appearance of the $\nu_b C{=}O$ band in the IRRAS spectra after each protonation step (Figure 5a). However at $\chi_{MUA}^{surf} = 0.15$, it is important to highlight that the $pK_{1/2}^{app}$ of the SAM at the first protonation step increases from 7.3 to 9.7 and the $\nu_b C{=}O$ band is absent until it appears once the second step is completed. This effect of the dilution in the interfacial properties of the SAM is probably due to an emerging population of MUA domains below a critical size where the local hydrophobicity predominates and hydrogen bonding is much less favoured than inside of the co-existing population of disordered MUA molecules arranged into domains still "large" enough.

Figure 7b shows a different scenario for the SAMs built at the longer time. A single $pK_{1/2}^{app}$ appears independently of their surface composition that turns to increase at higher MUA surface contents than it does for the SAMs formed at shorter times. At $\chi_{MUA}^{surf} < 0.60$, these mixed SAMs have readily achieved a sufficient population of MUA domains below a critical size that allows the effect of the low dielectric surrounding environment to quickly prevail in their interfacial properties and the $pK_{1/2}^{app}$ to displace to alkaline values of ~9.1-9.4 (Table 1). This confirms the results obtained by EIS titration that agrees with a mixing behaviour of both components closer to an ideal homogeneous distribution down to the molecular level. In this scenario, surface

groups might arrange in small groups of a few molecules, as dimers and/or totally isolated being all surrounded by quite similar environments. Finally, it is again observed at Figure 5b that the –COOH groups rearrange to form intermolecular hydrogen bonds even for those mixed SAMs ($\chi_{MUA}^{surf} < 0.60$) with a homogeneous distribution of MUA domains below a critical size. In this case, the existence of strong ionic hydrogen bonds should not be discarded as their formation is favoured, most likely in small groups of MUA molecules or dimers than between isolated moieties closely placed, under low ionic strength conditions such as in this work.[53, 65]

It has been demonstrated that the acid/base properties of homogeneously mixed SAMs of MUA and DT are influenced by changes in their surface patterning and structural organization. Consequently, the interfacial behavior of these SAMs according to its pattern design determines their possible applications. In this sense, the MUA/DT SAMs built at the shorter time are more versatile to mimic interactions with biomolecules at physiological pH. This is based on the wide percentage of $–COO^-$ and COOH surface groups (8-50 %) that is available to evaluate the effect of electrostatic and hydrogen bonding interactions as well as that of the hydrophobic ones by tuning the insertion of $–CH_3$ groups within a 10 to 85 % of the surface content. On the other hand, the MUA/DT mixed SAMs whose interfacial behavior is closer to that expected for molecularly patterned surfaces better meet the requirements of organic electronics based on junctions where the interfacial transport physics would be tailored through well-defined gradients of rectification by finely tuning their surface chemistry. However, the structural robustness seems still an issue as defects are progressively induced by the reorganization of the SAMs during their titration due to acid/base surface reactions.

Conclusions

The acid/base interfacial behavior of MUA/DT SAMs depends on the degree of homogeneous mixing and spatial distribution of both components arranging into different patterns as a function of their surface composition. EIS and IR titration curves clearly show the change in the degree of the dissociation of the –COOH groups in pure MUA and mixed MUA/DT SAMs on Au. The fitting of experimental data to the 1-pK model allows determining the apparent surface $pK_{1/2}^{app}$, the intrinsic pK_a and the interaction parameter, $\beta\overline{E}$, values as a function of the surface composition of the SAMs. The values and evolution of these parameters suggest that the interfacial properties of the SAMs are not only influenced by their repulsive intermolecular interactions but also by hydrogen bonding, ion solvation and hydrophobic effects that would be present in the vicinity of the ionizable end-groups confined in the surface.

Firstly, the appearance of a single $pK_{1/2}^{app}$ that initially decreases upon dilution of MUA with DT is consistent with the lowering of the in-plane repulsive interactions between ionizable groups which experiment a similar local environment to that of the pure MUA SAM. This acid/base interfacial behavior is typical of SAMs homogeneously mixed at the nanoscale. Secondly, when MUA domains decrease below a critical size the effect of lowering of the local dielectric constant predominates in the vicinity of the groups. The transition between both scenarios is determined by the heterogeneity in the size distribution of MUA and DT nanodomains at the SAMs. A higher heterogeneity explains the appearance of two $pK_{1/2}^{app}$ in the IR titration curves due to the coexistence of different local environments created by –COOH groups arranged in smaller and larger MUA domains. The –COOH located in small groups or at $–CH_3$ domain boundaries contribute with a higher $pK_{1/2}^{app}$, while those located inside of larger MUA domains are titrated at the lower $pK_{1/2}^{app}$. On the other hand, the SAMs closer to an ideal molecular mixing

have a single $pK_{1/2}^{app}$ that shifts to alkaline values at lower MUA surface contents. This acid/base behavior is a consequence of the similar local microenvironments experienced by all the surface groups which are assumed to be distributed in very small groups, as dimers or even isolated.

Finally, hydrogen bonding interactions between MUA molecules is observed upon the rearrangement of the SAM structure. It is suggested that dimeric species are most likely to form by association of MUA molecules either inside of the larger domains or as pre-existing dimers homogeneously mixed in the surface.

Acknowledgements

We thank the Ministerio de Economía y Competitividad (MINECO) (Projects CTQ2014-60227-R and CTQ-2015–71955-REDT Network of excellence Sensors and Biosensors), Junta de Andalucía (P10-FQM-6408) and University of Córdoba for financial support of this work.

References

1. Smith, R. K.; Lewis, P. A.; Weiss, P. S., Patterning Self-Assembled Monolayers. *Prog. Surf. Sci.* **2004,** *75*, 1-68.

2. Claridge, S. A.; Liao, W.-S.; Thomas, J. C.; Zhao, Y.; Cao, H. H.; Cheunkar, S.; Serino, A. C.; Andrews, A. M.; Weiss, P. S., From the Bottom Up: Dimensional Control and Characterization in Molecular Monolayers. *Chem. Soc. Rev.* **2013,** *42*, 2725-2745.

3. Casalini, S.; Bortolotti, C. A.; Leonardi, F.; Biscarini, F., Self-Assembled Monolayers in Organic Electronics. *Chem. Soc. Rev.* **2017,** *46*, 40-71.

4. Majumdar, S.; Malen, J. A.; McGaughey, A. J. H., Cooperative Molecular Behavior Enhances the Thermal Conductance of Binary Self-Assembled Monolayer Junctions. *Nano Lett.* **2017,** *17*, 220-227.

5. Kong, G. D.; Kim, M.; Cho, S. J.; Yoon, H. J., Gradients of Rectification: Tuning Molecular Electronic Devices by the Controlled Use of Different-Sized Diluents in Heterogeneous Self-Assembled Monolayers. *Angew. Chem., Int. Ed.* **2016,** *55*, 10307-10311.

6. Puente Santiago, A. R.; Pineda, T.; Blazquez, M.; Madueno, R., Formation of 2-D Crystalline Intermixed Domains at the Molecular Level in Binary Self-Assembled Monolayers from a Lyotropic Mixture. *Journal of Physical Chemistry C* **2016,** *120*, 8595-8606.

7. Bain, C. D.; Whitesides, G. M., Modeling Organic Surfaces with Self-Assembled Monolayers. *Angew. Chem.* **1989,** *101*, 522-8.

8. Bain, C. D.; Evall, J.; Whitesides, G. M., Formation of Monolayers by the Coadsorption of Thiols on Gold - Variation in the Head group, Tail Group, and Solvent. *J. Am. Chem. Soc.* **1989,** *111*, 7155-7164.

9. Colangelo, E.; Comenge, J.; Paramelle, D.; Volk, M.; Chen, Q.; Levy, R., Characterizing Self-Assembled Monolayers on Gold Nanoparticles. *Bioconjugate Chem.* **2017,** *28*, 11-22.

10. Mendes, P. M., Stimuli-Responsive Surfaces for Bio-Applications. *Chem. Soc. Rev.* **2008,** *37*, 2512-2529.

11. Yang, H.; Yuan, B.; Zhang, X.; Scherman, O. A., Supramolecular Chemistry at Interfaces: Host-Guest Interactions for Fabricating Multifunctional Biointerfaces. *Acc. Chem. Res.* **2014,** *47*, 2106-2115.

12. Jacquelin, D. K.; Perez, M. A.; Euti, E. M.; Arisnabarreta, N.; Cometto, F. P.; Paredes-Olivera, P.; Patrito, E. M., A pH-Sensitive Supramolecular Switch Based on Mixed Carboxylic Acid Terminated Self-Assembled Monolayers on Au(111). *Langmuir* **2016,** *32*, 947-953.

13. Prime, K. L.; Whitesides, G. M., Self-Assembled Organic Monolayers: Model Systems for Studying Adsorption of Proteins at Surfaces. *Science* **1991,** *252*, 1164.

14. Gooding, J. J.; Darwish, N., The Rise of Self-Assembled Monolayers for Fabricating Electrochemical Biosensors-An Interfacial Perspective. *Chem. Rec.* **2012,** *12*, 92-105.

15. Frasconi, M.; Mazzei, F.; Ferri, T., Protein Immobilization at Gold-Thiol Surfaces and Potential for Biosensing. *Anal. Bioanal. Chem.* **2010,** *398*, 1545-1564.

16. Arya, S. K.; Solanki, P. R.; Datta, M.; Malhotra, B. D., Recent Advances in Self-Assembled Monolayers Based Biomolecular Electronic Devices. *Biosens. Bioelectron.* **2009,** *24*, 2810-2817.

17. Biju, V., Chemical Modifications and Bioconjugate Reactions of Nanomaterials for Sensing, Imaging, Drug Delivery and Therapy. *Chem. Soc. Rev.* **2014,** *43*, 744-764.

18. Dennis, A. M.; Delehanty, J. B.; Medintz, I. L., Emerging Physicochemical Phenomena along with New Opportunities at the Biomolecular-Nanoparticle Interface. *J. Phys. Chem. Lett.* **2016,** *7*, 2139-2150.

19. Samanta, D.; Sarkar, A., Immobilization of Bio-Macromolecules on Self-Assembled Monolayers: Methods and Sensor Applications. *Chem Soc Rev* **2011,** *40*, 2567-92.

20. Fedurco, M., Redox Reactions of Heme-Containing Metalloproteins: Dynamic Effects of Self-Assembled Monolayers on Thermodynamics and Kinetics of Cytochrome c Electron-Transfer Reactions. *Coordination Chemistry Reviews* **2000,** *209*, 263-331.

21. Jin, B.; Wang, G.-X.; Millo, D.; Hildebrandt, P.; Xia, X.-H., Electric-Field Control of the pH-Dependent Redox Process of Cytochrome c Immobilized on a Gold Electrode. *J. Phys. Chem. C* **2012,** *116*, 13038-13044.

22. Chen, S.; Liu, L.; Zhou, J.; Jiang, S., Controlling Antibody Orientation on Charged Self-Assembled Monolayers. *Langmuir* **2003,** *19*, 2859-2864.

23. Hamelin, A., Cyclic Voltammetry at Gold Single-Crystal Surfaces. Part 1. Behavior at Low-Index Faces. *J. Electroanal. Chem.* **1996,** *407*, 1-11.

24. Trasatti, S.; Petrii, O. A., Real Surface-Area Measurements in Electrochemistry. *Pure and Applied Chemistry* **1991,** *63*, 711-734.

25. Janek, R. P.; Fawcett, W. R.; Ulman, A., Impedance Spectroscopy of Self-Assembled Monolayers on Au(111): Sodium Ferrocyanide Charge Transfer at Modified Electrodes. *Langmuir* **1998,** *14*, 3011-3018.

26. Garcia-Raya, D.; Madueno, R.; Manuel Sevilla, J.; Blazquez, M.; Pineda, T., Electrochemical Characterization of a 1,8-Octanedithiol Self-Assembled Monolayer (ODT-SAM) on a Au(111) Single Crystal Electrode. *Electrochimica Acta* **2008,** *53*, 8026-8033.

27. Kim, K.; Kwak, J., Faradaic Impedance Titration of Pure 3-Mercaptopropionic Acid and Ethanethiol Mixed Monolayers on Gold. *J. Electroanal. Chem.* **2001,** *512*, 83-91.

28. Sanders, W.; Vargas, R.; Anderson, M. R., Characterization of Carboxylic Acid-Terminated Self-Assembled Monolayers by Electrochemical Impedance Spectroscopy and Scanning Electrochemical Microscopy. *Langmuir* **2008,** *24*, 6133-6139.

29. Pissinis, D. E.; Linarez Perez, O. E.; Cometto, F. P.; Lopez Teijelo, M., Preparation and Characterization of Self Assembled Monolayers of 2-Mercaptonicotinic Acid on Au(1 1 1). *J. Electroanal. Chem.* **2014,** *712*, 167-177.

30. Yan, Y.; Zheng, Q.; Yang, Y.; Liu, Y.; Shao, H., Regulating the Electrochemical Reversibility of $Fe(CN)_6^{3-/4-}$ by Altering the Surface Potential of the Compact Layer. *J. Electrochem. Soc.* **2016,** *163*, H982-H987.

31. Becka, A. M.; Miller, C. J., Electrochemistry at omega-Hydroxy Thiol coated Electrodes - A Comparison of the Double Layer at omega-Hydroxy Thiol and Alkanethiol Monolayer coated Au Electrodes. *J. Phys. Chem.* **1993,** *97*, 6233-6239.

32. Komura, T.; Yamaguchi, T.; Shimatani, H.; Okushio, R., Interfacial Charge-Transfer Resistance at Ionizable Thiol Monolayer-Modified Gold Electrodes as Studied by Impedance Spectroscopy. *Electrochim. Acta* **2004,** *49*, 597-606.

33. Madueno, R.; Garcia-Raya, D.; Viudez, A. J.; Sevilla, J. M.; Pineda, T.; Blazquez, M., Influence of the Solution pH in the 6-Mercaptopurine Self-Assembled Monolayer (6MP-SAM) on a Au(111) Single-Crystal Electrode. *Langmuir* **2007,** *23*, 11027-11033.

34. Molinero, V.; Calvo, E. J., Electrostatic Interactions at Self Assembled Molecular Films of Charged Thiols on Gold. *J. Electroanal. Chem.* **1998,** *445*, 17-25.

35. White, H. S.; Peterson, J. D.; Cui, Q.; Stevenson, K. J., Voltammetric Measurement of Interfacial Acid/Base Reactions. *J. Phys. Chem. B* **1998,** *102*, 2930-2934.

36. Kakiuchi, T.; Iida, M.; Imabayashi, S.-i.; Niki, K., Double-Layer-Capacitance Titration of Self-Assembled Monolayers of ω-Functionalized Alkanethiols on Au(111) Surface. *Langmuir* **2000,** *16*, 5397-5401.

37. Xing, Y. F.; Li, S. F. Y.; Lau, A. K. H.; O'Shea, S. J., Electrochemical Impedance Spectroscopy Study of Mixed Thiol Monolayers on Gold. *J. Electroanal. Chem.* **2005,** *583*, 124-132.

38. Niu, L.; Kvarnstroem, C.; Ivaska, A., Evaluation of Coverage of Self-Assembled Polyaniline-Analogue Monolayer by Capacitance Measurements. *J. Electroanal. Chem.* **2007,** *600*, 95-102.

39. Widrig, C. A.; Chung, C.; Porter, M. D., The Electrochemical Desorption of n-Alkanethiol Monolayers from Polycrystalline Au and Ag Electrodes. *Journal of Electroanalytical Chemistry and Interfacial Electrochemistry* **1991,** *310*, 335-359.

40. Porter, M. D.; Bright, T. B.; Allara, D. L.; Chidsey, C. E. D., Spontaneously Organized Molecular Assemblies. 4. Structural Characterization of n-Alkyl Thiol Monolayers on Gold by Optical Ellipsometry, Infrared Spectroscopy, and Electrochemistry. *J. Am. Chem. Soc.* **1987,** *109*, 3559-3568.

41. Slowinski, K.; Chamberlain, R. V., II; Bilewicz, R.; Majda, M., Evidence for Inefficient Chain-to-Chain Coupling in Electron Tunneling through Liquid Alkanethiol Monolayer Films on Mercury. *J. Am. Chem. Soc.* **1996,** *118*, 4709-10.

42. Gonzalez-Granados, Z.; Sanchez-Obrero, G.; Madueno, R.; Sevilla, J. M.; Blazquez, M.; Pineda, T., Formation of Mixed Mono layers from 11-Mercaptoundecanoic Acid and Octanethiol on Au(111) Single Crystal Electrode under Electrochemical Control. *Journal of Physical Chemistry C* **2013,** *117*, 24307-24316.

43. Garcia-Raya, D.; Madueno, R.; Blazquez, M.; Pineda, T., Formation of 1,8-Octanedithiol Mono- and Bilayers under Electrochemical Control. *J. Phys. Chem. C* **2010,** *114*, 3568-3574.

44. Miller, C.; Cuendet, P.; Gratzel, M., Adsorbed omega-Hydroxy Thiol Monolayers on Gold Electrodes - Evidence for Electron-Tunneling to Redox Species in Solution. *J. Phys. Chem.* **1991,** *95*, 877-886.

45. Borkovec, M., Origin of 1-pK and 2-pK Models for Ionizable Water-Solid Interfaces. *Langmuir* **1997,** *13*, 2608-2613.

46. Gershevitz, O.; Sukenik, C. N., In Situ FTIR-ATR Analysis and Titration of Carboxylic Acid-Terminated SAMs. *J. Am. Chem. Soc.* **2004,** *126*, 482-483.

47. Tominaga, M.; Maetsu, S.; Kubo, A.; Taniguchi, I., Nano-Ordered Topographical Effects on Dissociation of Carboxylic Acid Terminated Self-Assembled Monolayers Adsorbed onto a Gold Surface. *J. Electroanal. Chem.* **2007,** *603*, 203-211.

48. Aureau, D.; Ozanam, F.; Allongue, P.; Chazalviel, J. N., The Titration of Carboxyl-Terminated Monolayers Revisited: In Situ Calibrated Fourier Transform Infrared Study of Well-Defined Monolayers on Silicon. *Langmuir* **2008,** *24*, 9440-9448.

49. Luque, A. M.; Cuesta, A.; Calvente, J. J.; Andreu, R., Potentiostatic Infrared Titration of 11-Mercaptoundecanoic Acid Monolayers. *Electrochem. Commun.* **2014,** *45*, 13-16.

50. Clark, R. A.; Trout, C. J.; Ritchey, L. E.; Marciniak, A. N.; Weinzierl, M.; Schirra, C. N.; Christopher Kurtz, D., Electrochemical Titration of Carboxylic Acid Terminated SAMs on Evaporated Gold: Understanding the Ferricyanide Electrochemistry at the Electrode Surface. *J. Electroanal. Chem.* **2013,** *689*, 284-290.

51. Ganesh, V.; Lakshminarayanan, V., Self-Assembled Monolayers of Alkanethiols on Gold Prepared in a Hexagonal Lyotropic Liquid Crystalline Phase of Triton X-100/Water System. *Langmuir* **2006,** *22*, 1561-1570.

52. Garcia Raya, D.; Madueno, R.; Blazquez, M.; Pineda, T., Formation of a 1,8-Octanedithiol Self-Assembled Monolayer on Au(111) Prepared in a Lyotropic Liquid-Crystalline Medium. *Langmuir* **2010,** *26*, 11790-11796.

53. Smith, D. A.; Wallwork, M. L.; Zhang, J.; Kirkham, J.; Robinson, C.; Marsh, A.; Wong, M., The Effect of Electrolyte Concentration on the Chemical Force Titration Behavior of ω-Functionalized SAMs: Evidence for the Formation of Strong Ionic Hydrogen Bonds. *J. Phys. Chem. B* **2000,** *104*, 8862-8870.

54. Creager, S. E.; Clarke, J., Contact-Angle Titrations of Mixed ω-Mercaptoalkanoic Acid/Alkanethiol Monolayers on Gold. Reactive vs Nonreactive Spreading, and Chain Length Effects on Surface pKa Values. *Langmuir* **1994,** *10*, 3675-83.

55. He, H.-X.; Huang, W.; Zhang, H.; Li, Q. G.; Li, S. F. Y.; Liu, Z. F., Demonstration of High-Resolution Capability of Chemical Force Titration via Study of Acid/Base Properties of a Patterned Self-Assembled Monolayer. *Langmuir* **2000,** *16*, 517-521.

56. Troughton, E. B.; Bain, C. D.; Whitesides, G. M.; Nuzzo, R. G.; Allara, D. L.; Porter, M. D., Monolayer Films Prepared by the Spontaneous Self-Assembly of Symmetrical and Unsymmetrical Dialkyl Sulfides from Solution onto Gold Substrates: Structure, Properties, and Reactivity of Constituent Functional Groups. *Langmuir* **1988,** *4*, 365-85.

57. Jiang, X.; Ataka, K.; Heberle, J., Influence of the Molecular Structure of Carboxyl-Terminated Self-Assembled Monolayer on the Electron Transfer of Cytochrome c Adsorbed on an Au Electrode: In Situ Observation by Surface-Enhanced Infrared Absorption Spectroscopy. *J. Phys. Chem. C* **2008,** *112*, 813-819.

58. Nuzzo, R. G.; Dubois, L. H.; Allara, D. L., Fundamental Studies of Microscopic Wetting on Organic Surfaces. 1. Formation and Structural Characterization of a Self-Consistent Series of Polyfunctional Organic Monolayers. *J. Am. Chem. Soc.* **1990,** *112*, 558-69.

59. Arnold, R.; Azzam, W.; Terfort, A.; Woell, C., Preparation, Modification, and Crystallinity of Aliphatic and Aromatic Carboxylic Acid Terminated Self-Assembled Monolayers. *Langmuir* **2002,** *18*, 3980-3992.

60. Hirata, N.; Suga, S.; Noguchi, Y.; Shibuta, M.; Tsunoyama, H.; Eguchi, T.; Nakajima, A., Highly Ordered Self-Assembled Monolayers of Carboxy- and Ester-Terminated Alkanethiols on Au(111): Infrared Absorption and Hyperthermal-Deposition Experiments with $Cr(benzene)_2$ Ions. *The Journal of Physical Chemistry C* **2017,** *121*, 6736-6747.

61. Sugihara, K.; Shimazu, K.; Uosaki, K., Electrode Potential Effect on the Surface pK_a of a Self-Assembled 15-Mercaptohexadecanoic Acid Monolayer on a Gold/Quartz Crystal Microbalance Electrode. *Langmuir* **2000,** *16*, 7101-7105.

62. Snyder, R. G.; Strauss, H. L.; Elliger, C. A., Carbon-Hydrogen Stretching Modes and the Structure of n-Alkyl Chains. 1. Long, Disordered Chains. *J. Phys. Chem.* **1982,** *86*, 5145-50.

63. Bethencourt, M. I.; Srisombat, L.-o.; Chinwangso, P.; Lee, T. R., SAMs on Gold Derived from the Direct Adsorption of Alkanethioacetates Are Inferior to Those Derived from the Direct Adsorption of Alkanethiols. *Langmuir* **2009,** *25*, 1265-1271.

64. de F. Paulo, T.; Abruna, H. D.; Diogenes, I. C. N., Thermodynamic, Kinetic, Surface pKa, and Structural Aspects of Self-Assembled Monolayers of Thio Compounds on Gold. *Langmuir* **2012,** *28*, 17825-17831.

65. Meot-Ner, M.; Elmore, D. E.; Scheiner, S., Ionic Hydrogen Bond Effects on the Acidities, Basicities, Solvation, Solvent Bridging, and Self-Assembly of Carboxylic Groups. *J. Am. Chem. Soc.* **1999,** *121*, 7625-7635.

66. Kane, V.; Mulvaney, P., Double-Layer Interactions between Self-Assembled Monolayers of ω-Mercaptoundecanoic Acid on Gold Surfaces. *Langmuir* **1998,** *14*, 3303-3311.

TOC Graphics